5-7-2009

Effects of Photointensity Gradient on Directional Crystal Growth in Blends of Crystalline Polymer and Photoreactive Monomer Undergoing Photopolymerization-Induced Phase Transformation

Pankaj Rathi

Soo Jeoung Park

Thein Kyu
University of Akron Main Campus, tkyu@uakron.edu

Effects of photointensity gradient on directional crystal growth in blends of crystalline polymer and photoreactive monomer undergoing photopolymerization-induced phase transformation

Pankaj Rathi, Soo Jeoung Park, and Thein Kyu[a)]
Department of Polymer Engineering, University of Akron, Akron, Ohio 44325, USA

(Received 13 February 2009; accepted 9 April 2009; published online 7 May 2009)

Effects of light intensity gradient on development of intricate hierarchical morphology of semicrystalline polyethylene oxide (PEO) and photoreactive diacrylate (DA) blends undergoing photopolymerization-induced crystallization have been demonstrated experimentally and theoretically. The melting temperature of PEO was found to decline upon addition of DA monomer. A solid-liquid phase diagram has been established by self-consistently solving the combined phase field free energy of crystal solidification and Flory–Huggins (FH) free energy of liquid-liquid demixing. Dynamic calculations were performed using time-dependent Ginzburg–Landau (model C) equations by incorporating the combined phase field and FH free energy densities coupled with the photopolymerization kinetics. The spatiotemporal development of gradient morphology was computed under various intensity gradient profiles including linear, cylindrical, and Gaussian profiles. The observed seaweed or dense lamellar branching morphology of the PEO/DA blend is strikingly similar to the directionally grown interface structures observed in metals driven by external thermal gradients. © *2009 American Institute of Physics*. [DOI: 10.1063/1.3126663]

I. INTRODUCTION

The phenomenon of reaction-induced phase separation (RIPS) has been extensively investigated for reactive polymer blends as a means of controlling the blend morphology.[1–3] The RIPS is a nonequilibrium and nonlinear process that involves the competition between the reaction kinetics and phase separation dynamics. The mechanism of RIPS has been attributed originally to a nucleation and growth (NG) mechanism, but this perception has been challenged.[4,5] Inoue[4] advocated the mechanism of spinodal decomposition (SD) during RIPS at the critical composition of a thermoplastic/thermoset blend. Upon polymerization in the isotropic state, the coexistence curve moves up, but it rarely crosses the reaction temperature at the critical point in most cases. Generally speaking, the coexistence curve crosses mostly at off-critical compositions, thus phase separation must be initiated in the metastable gap where NG is expected to occur. With the progression of the reaction, the system is further pushed into the unstable gap in which the mechanism of RIPS is dominated by the SD process, and thus the crossover occurs from the NG with a dispersed morphology to the SD with a bicontinuous structure. This crossover behavior of RIPS is coined as nucleation initiated SD for a blend of liquid rubber/epoxy.[5] More importantly, the supercooling, i.e., the temperature difference between a snapshot coexistence curve and a reaction temperature, becomes larger with continued polymerization that in turn reduces the length scale (or domain size). Such tendency of domain size reduction is an important feature particularly for improvement of physical and mechanical properties of toughened plastics and polymer networks.[1–3]

While the phenomenon of polymerization-induced phase separation is well explored for thermoplastic/thermoset composites[1–5] and polymer dispersed liquid crystal systems,[6–8] polymerization-induced crystallization in crystalline polymer blends is relatively new.[9] Recently, a novel phenomenon of photopolymerization-induced crystallization (PIC) was reported by Park *et al.*[9] for the blends of semicrystalline polyethylene oxide (PEO) and diacrylate (DA) blends. It was shown that the melting temperature of PEO was lowered upon addition of DA due to the plasticization effect resulting from the interaction between the crystalline polymer and the diluent. Upon photopolymerization, the reactive DA monomer is converted into polymer through free radical photopolymerization, the melting temperature of PEO rises as the system attempts to restore its pure state value. By the time the melting point curve surpasses the reaction temperature, crystallization is triggered showing the temporal emergence of polymer crystals such as needlelike lamellae evolving to spherulites. This phenomenon is called polymerization-induced crystallization. In addition, Park *et al.*[9] found experimentally that directional crystal growth occurred in the PEO/DA blends due to the intensity gradient of the irradiated beam. The observed seaweed or dense lamellar branching morphology is strikingly similar to the directionally grown interface structures observed in metals driven by external thermal gradients.[10,11]

In the present paper, a theoretical model is introduced for photopolymerization-induced phase transformation in the crystalline blends subjected intensity gradient by combining Flory–Huggins (FH) theory of liquid-liquid mixing[12] with

[a)]Author to whom correspondence should be addressed. Electronic mail: tkyu@uakron.edu.

the phase field model of crystallization[13–17] by taking into consideration crystalline-amorphous interaction between the constituents.[18] The coexistence curves of the upper critical solution temperature (UCST) were established by solving self-consistently. Subsequently, the snapshot coexistence curves were calculated by self-consistently solving a set of reaction-diffusion equations based on time-dependent Ginzburg–Landau (TDGL) (model C) equations by incorporating the combined phase field free energy density for crystal solidification and FH free energy density for liquid-liquid demixing coupled with the photopolymerization kinetics under the assumption that the system reaches equilibrium at each conversion step.

To compare with the calculated crystal-phase morphologies, PIC of the PEO/DA blend was carried out using optical microscopy under various intensity gradient profiles of defocused illuminating beams. The directional crystal growth of PEO was seen under a linear intensity gradient beam as well as circular and Gaussian intensity profiles with varying interface sharpness. Of particular interest is the computed crystalline textures accord reasonably well to the experimental observations of the PEO/DA system.

II. THEORETICAL MODEL

The free energy density of a polymer system (f) containing crystalline polymer and reactive constituent consists of three terms: (i) FH free energy density of liquid-liquid demixing, (ii) phase field free energy density of crystallization given by the Landau-type double well potential, and (iii) coupling free energy density representing the interaction between amorphous and crystalline phases,[18]

$$f(\psi,\phi) = f_{\text{mixing}} + \phi_i f_{\text{crystal}} + f_{\text{coupling}}, \tag{1}$$

where ϕ and ψ are the concentration order parameter (i.e., volume fraction) and the crystal order parameter, respectively. The FH free energy density of mixing for a crystalline polymer/reactive monomer blend[19] may be expressed as

$$f_{\text{mixing}} = f(\phi) = \frac{\phi_1 \ln \phi_1}{r_1} + \frac{\phi_2 \ln \phi_2}{r_2} + \chi_{\text{FH}}\phi_1\phi_2, \tag{2}$$

where ϕ_1 and ϕ_2 are volume fractions of the crystalline polymer and monomer constituents, respectively, under the incompressibility condition $\phi_1+\phi_2=1$ and $\chi_{\text{FH}}=\chi_{aa}=A+B/T$ is the FH interaction parameter with A being entropic correction and $B=(\chi_c-A)T_c$, in which χ_c is the critical FH interaction parameter at the critical temperature T_c. The parameters r_1 and r_2 are the number of statistical segments or the lattice sites occupied by the macromolecule and the reactive monomer, respectively.

The phase field free energy of crystallization is given by a Landau-type double well potential pertaining to the crystal order parameter ψ_i,[18]

$$f_{\text{crystal}} = f(\psi_i) = W_i\left(\frac{\zeta_i\zeta_{i,0}}{2}\psi_i^2 - \frac{\zeta_i+\zeta_{i,0}}{3}\psi_i^3 + \frac{1}{4}\psi_i^4\right), \tag{3}$$

where W_i is a coefficient representing the energy barrier for nucleation and ψ_i is the crystal order parameter for each constituent. Subscript i represents crystalline polymer (i.e., component 1) and reactive monomer (i.e., component 2), respectively. The potential well at $\psi_1=0$ indicates the metastable melt of the crystalline polymer and $\psi_1=\zeta_{1,0}$ refers to the stable crystalline state with ζ_1 being the free energy barrier for the crystal nucleation to overcome. The crystal order parameter of the polymer crystal, ψ_1, is defined as $\psi_1=\ell/\ell^0$, where ℓ is the lamellar thickness and ℓ^0 is that of the perfect polymer crystal and thus their ratio represents the linear crystallinity (i.e., one dimensional crystallinity).[18] For a small molecule system, the crystal order parameter at the crystallization potential is taken as unity, i.e., $\psi_i=\zeta_{i,0}=1$. The solidification potential at a given crystallization temperature, T_x, is $\zeta_0=(T_m^0-T_m)/(T_m^0-T_x)$, where T_m^0 is the equilibrium melting temperature and T_m the crystal melting temperature of crystalline polymer upon crystallization at T_x.[16,17] The free energy penalty representing the solidification hump (barrier), W_i is related to the heat of fusion, $\Delta H_{u,i}$ and ζ_i as follows:

$$W_i = \frac{6\Delta H_{u,i}}{RT}\left(1-\frac{T}{T_{m,i}^0}\right)\left(\frac{1}{2}-\zeta_i\right)^{-1}, \tag{4}$$

where R is the gas constant and the two bracket terms signify correction for the supercooling effects.

The coupling free energy representing the interaction between two crystalline constituents is given as

$$f_{\text{coupling}} = \phi_1\phi_2(\chi_{ca}\psi_1^2 - \chi_{cc}\psi_1\psi_2 + \chi_{ac}\psi_2^2), \tag{5}$$

where χ_{ca} represents the interaction between the crystal of the first constituent and the amorphous of the second constituent, i.e., $\chi_{c_1a_2}=\chi_{ca}$, which is hereafter termed as the crystalline-amorphous interaction parameter.[18] The term $\phi_1\psi$ represents the bulk crystallinity of the polymer with volume fraction ϕ_1, whereas $\psi\phi_2$ signifies the interaction of the crystals with the surrounding monomer $\phi_2=\phi_m$; hence the term $\chi_{ca}\phi_1\psi\phi_2\psi$ represents the free energy of crystalline-amorphous interaction.[18] Further, the cross interaction within the cocrystals may be given by their geometric means, i.e., $\chi_{cc}=c_\omega\sqrt{\chi_{ca}\chi_{ac}}$. Hence, the local free energy of the blend containing a crystalline polymer and a reactive monomer can be given as

$$\begin{aligned} f(\psi_i,\phi) = {} & \frac{\phi_1 \ln \phi_1}{r_1} + \frac{\phi_2 \ln \phi_2}{r_2} + \chi_{aa}\phi_1\phi_2 \\ & + W_i\phi_i\left(\frac{\zeta_i\zeta_{i,0}}{2}\psi_i^2 - \frac{\zeta_i+\zeta_{i,0}}{3}\psi_i^3 + \frac{1}{4}\psi_i^4\right) \\ & + \phi_1\phi_2(\chi_{ca}\psi_1^2 - \chi_{cc}\psi_1\psi_2 + \chi_{ac}\psi_2^2), \end{aligned} \tag{6}$$

where $\chi_{\text{FH}}=\chi_{aa}$ representing amorphous-amorphous interaction of the pair in the melt state. Note that the free energy of crystallization is weighted by the volume fraction of each crystalline constituent to account for the crystallinity in the blends.[18]

III. CONSTRUCTION OF THE PHASE DIAGRAMS

Prior to calculating the coexistence lines, it is important to first determine the solid-liquid phase transition by minimizing the free energy with respect to the crystal order parameter, ψ_1,

$$\frac{\partial f}{\partial \psi_1} = \phi_1 W_1[\psi_1^3 - (\zeta_1 + \zeta_{1,0})\psi_1^2 + \zeta_1\zeta_{1,0}\psi_1] + 2\phi_1\phi_2[\chi_{ca}\psi_1 - \chi_{cc}\psi_2] = 0, \quad (7)$$

which gives the equilibrium values of the crystal order parameter ψ_1 for each composition of the blend ϕ_1. In binary crystalline polymer systems, χ_{cc} is negligibly small since cocrystal is a rare occurrence, and thus this term may be ignored. At the melting temperature of component 1, component 2 is practically in the melt state and thus the blend can be treated as a polymer/diluent system. At equilibrium, the free energy pertaining to the crystal order parameter is also zero, i.e., $f(\psi_1)=0$, leading to

$$W_1\left[\frac{\psi_1^2}{4} - (\zeta_1 + \zeta_{1,0})\frac{\psi_1}{3} + \frac{\zeta_1\zeta_{1,0}}{2}\right] + \chi_{ca}\phi_2 = 0,$$

where $\psi_1 \simeq \zeta_{1,0}$ and $\zeta_{1,0} \simeq 1$ at equilibrium. Combining with Eq. (4), one obtains $1 - T_{m,1}/T_{m,1}^0 = (RT_{m,1}/\Delta H_{u,1})\phi_2\chi_{ca}$, which in turn results in $\chi_{ca} = B_{c,1}\Delta H_{u,1}/RT$ with $B_{c,1} = (1 - T_{1,m}/T_{1,m}^0)/\phi_2$.[19] As demonstrated by Rathi *et al.*,[19] χ_{ca} value can be determined experimentally from the melting point depression versus concentration (or volume fraction) of diluent plot.

To determine the value of χ_{ac}, a similar free energy minimization may be performed with respect to ψ_2 for the second crystalline constituent. However, the first component is practical in the solid state, showing little or no melting point depression and thus it may be estimated in accordance with $\chi_{ac} = B_{c,2}\Delta H_{u,2}/RT$. The minimized values of ψ_i thus obtained may be subsequently substituted in the free energy expression [Eq. (6)] and then the coexistent points may be calculated by balancing the pseudo chemical potentials for each phase, viz., $(\partial f/\partial \phi_i)|_{\phi_i^\alpha} = (\partial f/\partial \phi_i)|_{\phi_i^\beta}$. The detailed procedures for seeking the self-consistent solution by a double tangent algorithm can be found elsewhere.[8,18]

IV. FREE ENERGY CHANGE DURING PHOTOPOLYMERIZATION

During the course of polymerization, the value of r_2 changes to r_P representing the number of statistical segments of the emerged polymer, under the constraint that $\phi_2 = \phi_m + \phi_P$. Assuming that the monomer and the polymer thus formed are completely miscible and have the same FH interaction parameter with respect to the crystalline counter part, Eq. (2) may be rewritten[9] as

$$f_{\text{mixing}} = f(\phi_i) = \frac{\phi_1 \ln(\phi_1)}{r_1} + \frac{\phi_m \ln(\phi_m)}{r_m} + \frac{\phi_P \ln(\phi_P)}{r_P} + \chi_{aa}\phi_1(1 - \phi_1), \quad (8)$$

assuming that the equilibrium is reached at each conversion and $r_m = 1$.

Now let us consider a binary crystalline polymer/crystallizable reactive monomer system such as PEO/DA blends.[9] During photopolymerization, DA monomers were transformed into the acrylate network, which in turn prevent crystallization of DA. The total free energy of such polymerizing system can then be simplified for each conversion step by setting $\psi_1 = \psi$ because PEO is the only component undergoing PIC. During the polymerization, monomer (ϕ_m) changes to polymer (ϕ_p) under the constraint that $\phi_1 + \phi_2 = 1$ with $\phi_m + \phi_p = \phi_2$, viz.,

$$f(\psi, \phi) = \frac{\phi_1 \ln(\phi_1)}{r_1} + \phi_m \ln(\phi_m) + \frac{\phi_P \ln(\phi_P)}{r_P} + \chi_{aa}\phi_1(1 - \phi_1) + W_1\phi_1\left(\frac{\zeta\zeta_0}{2}\psi^2 - \frac{\zeta + \zeta_0}{3}\psi^3 + \frac{1}{4}\psi^4\right) + \chi_{ca}\phi_1\phi_2\psi^2. \quad (9)$$

Once polymerization reaction is triggered in the DA, the PEO/DA blend can be treated as a crystalline PEO—amorphous DA solution,[9] and thus Eq. (9) is adequate for describing the polymerization-induced crystallization of PEO/DA blends under consideration.

V. PHOTOPOLYMERIZATION KINETICS

The nonequilibrium snapshots of the phase diagram during the course of polymerization reaction were calculated using the instantaneous volume fractions of the monomer and the polymer formed from it, viz.,

$$\alpha = \frac{\phi_2 - \phi_m}{\phi_2}, \quad \phi_P = \alpha\phi_2, \quad \text{or} \quad \phi_m = (1 - \alpha)\phi_2, \quad (10)$$

where α is conversion of monomers into a polymer. The rate of conversion is given by the first order reaction given as

$$\frac{d\alpha}{dt} = k(1 - \alpha) = k(\phi_m/\phi_2). \quad (11)$$

In actual photopolymerization, the lumped rate constant k is given as the ratio of the propagation and n-power of the termination rate constants, i.e., $k = k_p/k_t^n$, where n is the reaction exponent; it is 0.5 under the assumption of the bimolecular termination reaction between macroradicals.[20–24]

According to the classical kinetic model,[20] the polymerization rate is treated to be proportional to the square root of I_a at equal monomer conversions as

$$-\frac{d[M]}{dt} = k[M][\Phi I_a]^m, \quad (12)$$

where m is the reaction exponent and the conversion rate is proportional to the one-half power of the intensity of irradiation, $I_a^{1/2}$. This assumption may be valid in the initial stage of the reaction, but at the steady state where termination via trapping is competing with termination by combination, the exponent m has a value of unity.[21] In practice, this exponent is not exactly unity, i.e., around 0.8–0.9; this departure from ideality suggests a complex mechanism of free radical photopolymerization such as radical trapping, cyclization, etc., which may be influenced by blend composition, monomer functionality, radiation dosage, among others.[24]

VI. DYNAMIC CALCULATIONS ON SPATIOTEMPORAL CRYSTAL GROWTH

As pointed out above, the DA will be treated as amorphous as crystallization of DA did not occur at the reaction

temperature and thus the dynamic calculation will be performed as the crystalline-amorphous system. The total free energy of such blend may be expressed in terms of the local [Eq. (9)] and nonlocal gradient contributions, viz.,

$$F = \int_V \left(f(\phi,\psi) + \frac{\kappa^{\phi_k}}{2}|\nabla\phi_k|^2 + \frac{\kappa^{\psi}}{2}|\nabla\psi|^2 \right) dV. \tag{13}$$

$\kappa^{\phi}=a_k^2/18\phi_k$ and κ^{ψ} are the coefficients of the interface gradients in the corresponding composition and crystal-phase order parameter fields, respectively, and a_k is the characteristic length. The dynamics of the photopolymerization-induced phase transitions may be calculated in the context of TDGL—model C (Ref. 10) by coupling the conserved concentration (or volume fraction) and the nonconserved crystal order parameters. The governing nonlinear reaction-diffusion equations may be described as follows:[8,9]

$$\frac{\partial\phi_1}{\partial t} = \nabla[\Lambda\,\nabla\,(\delta F/\delta\phi_1)] + \eta, \tag{14}$$

$$\frac{\partial\phi_m}{\partial t} = \nabla[\Lambda\,\nabla\,(\delta F/\delta\phi_m)] - \dot{\alpha}\phi_m, \tag{15}$$

$$\frac{\partial\psi}{\partial t} = -\Gamma^{\psi}\frac{\delta F}{\delta\psi}, \tag{16}$$

where Λ is the mutual diffusion coefficient represented by the Onsager-type mobility as $1/\Lambda=(\phi_1/\Lambda_1)+(\phi_m/\Lambda_m)+(\phi_p/\Lambda_p)$ and $\Lambda_k=D_k r_k \phi_k^2$, where D_k is the translational diffusion coefficient and r_k is the number of statistical segments. It can be anticipated that the mobility changes with changing blend compositions during polymerization. Γ^{ψ} represents the mobility in the crystal order parameter field and η indicates the thermal noise that satisfies the fluctuation-dissipation theorem. $\delta/\delta\phi=\partial/\partial\phi-\nabla(\partial/\partial\nabla\phi)$ is the functional derivative and $\dot{\alpha}$ is the rate of conversion. Equations (14) and (15) are further coupled to the energy conservation equation,

$$\frac{\partial T}{\partial t} = \theta\nabla^2 T + K\frac{\partial\psi}{\partial t} + \frac{\Delta H_P}{\rho C_P}\dot{\alpha}\phi_m, \tag{17}$$

where $\theta=k_T/\rho C_P$ is thermal diffusivity in which C_p is heat capacity, ρ is density, k_T is thermal conductivity of the material, and ΔH_u is the latent heat (or heat of fusion of the crystal). In addition, ΔH_P is heat of polymerization liberated during the conversion of monomer to the polymer. Equations (14)–(16) are simultaneously solved in dimensionless units (signified by the tilde sign) viz., $\tilde{\nabla}=\nabla/a$, $\tilde{t}=tD/a^2$, $\widetilde{\kappa^{\psi}}=\kappa^{\psi}/a^2$, and $\widetilde{\Gamma^{\psi}}=\Gamma^{\psi}a^2/D$ according to Eq. (17), where a and D are the characteristic length scale and the translational diffusion coefficient, respectively.

VII. COMPUTATION SCHEME

Various intensity profiles such as linear, circular, and Gaussian were developed by setting the conversion rate to be proportional to the square root of the incident intensity. For a linear intensity gradient,

$$I = I_{\min} + (I_{\max} - I_{\min})\frac{x}{X}, \tag{18}$$

where $I_{\min}$ and $I_{\max}$ are minimum and maximum intensity values of the linear gradient filter, respectively. x is the grid number starting from the lowest intensity side and X is the frame size of 500. In the case of a circular profile (flattop view of the cylindrical beam), the boundary conditions may be set as

$$\begin{aligned} &I = I_{\max}, \quad r < 2R/3, \\ &I = I_{\min}, \quad 2R/3 < r < R, \end{aligned} \tag{19}$$

where r is a radial distance from the center and R is the radius of the illuminating beam. In the case of a Gaussian beam profile, the intensity profile takes the following form, viz.,

$$I = (I_{\max} - I_{\min})\exp(-r^2/3R^2). \tag{20}$$

The two dimensional (2D) calculations of morphology development were performed using a second order central difference scheme in space and a forward difference scheme in time with a (500×500) square grid in units of μm^2 under no-flux (or Neumann) boundary conditions.

VIII. RESULTS AND DISCUSSION

Prior to studying the effect of photointensity gradient on the crystallization in polymer blends, it is important to determine the phase diagram of the starting crystalline/reactive monomer blends in order to provide guidance to the pathway for the polymerization-induced phase transformation. In order to determine the crystal-liquid (melt) phase transition of the constituents, the free energy [i.e., Eq. (9)] was first minimized with respect to the individual crystal order parameters for each temperature using the free energy penalty representing the solidification hump (barrier), W related to the heat of fusion, ΔH_u as

$$W_i = (6\Delta H_{u,i}/RT)(1 - T/T^0_{m,i})(1/2 - \zeta_i)^{-1}, \tag{21}$$

where R is the gas constant and the last two bracket terms signify correction for the supercooling effects. At equilibrium, W_i is reduced to $W_i=6\Delta H_{u,i}/RT$. In the calculation of the nonequilibrium and nonlinear dynamics, Eq. (21) must be used. To determine the coexistent points, the equilibrium value of the crystal order parameter, ψ_ι, thus minimized for each blend composition (ϕ_ι) was subsequently substituted in the free energy expression of Eq. (9) and then the pseudochemical potentials at each phase were balanced, viz., $\partial f_i/\partial\phi_\iota|_{\phi_\iota^\alpha} = \partial f_i/\partial\phi_\iota|_{\phi_\iota^\beta}$. Subsequently, the coexistence curves were determined using a common tangent algorithm; the detailed description of the aforementioned approach may be found elsewhere.[18]

The solid-liquid phase diagram of PEO/DA blend obtained by differential scanning calorimetry is depicted in Fig. 1, exhibiting the coexistence of a solid crystal (Cr_1)+liquid (L_2) gap.[25,26] Various parameters used in the calculations are presented in Table I. Nonequilibrium snapshots of the phase diagram were calculated at various monomer conversions.

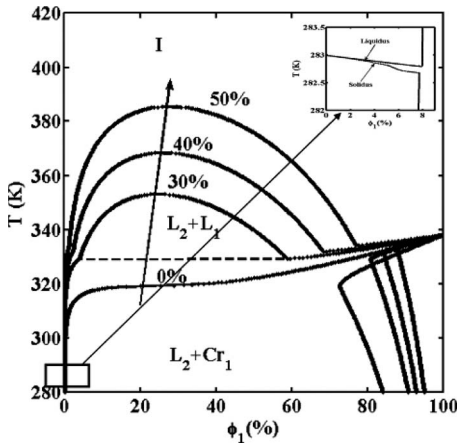

FIG. 1. Phase diagram showing lowering of the melting temperature of the crystalline PEO upon blending with the photoreactive DA monomer. Nonequilibrium snapshots of the coexistence curves were calculated at each conversion of DA monomer into the polymer subjected to photopolymerization. Various parameters used for the calculation of the phase diagram of PEO/DA blends were $r_1=110$, $r_2=1$, $T_m=338$ *K*, $\chi_{ca}=0.27$, and $\chi_{aa}=0.0134$ at $T_r=323$ *K*.

During polymerization, the molecular weight of the reactive monomer in the blend increased and thus the miscibility between the blending components was reduced resulting in the straightening of the melting point curve while the melting point of the crystalline component tried to restore its pure state value. When the restoring melting point exceeds the reaction temperature, crystallization takes place. Concurrently, the UCST envelope was pushed up leading to liquid (L_1)—liquid (L_2) phase separation in the melt.

When the PEO/DA system is subjected to a light intensity gradient, the conversion of the DA monomer is different for each local concentration, and thus the supercooling, i.e., the driving force for crystallization and phase separation, is different from location to location. This variance in the driving force caused by the nonuniform intensity distribution leads to the directional crystal growth in such photopolymerizing systems. Note that the dynamic computations were carried out at the isotropic state slightly above the liquidus line, indicated by the × symbol. In the simulations of morphology development, a square 2D grid (500×500) was used that corresponded to 500×500 μm^2. A second order central difference scheme in space and a forward difference scheme in time were employed under a periodic boundary condition for both the composition order as well as the crystal order parameter field. The emerging patterns of each field were solved in dimensionless renormalized parameters: $\Gamma^{\psi}=10$, $\Lambda_{\phi}=0.1$, $\kappa^{\psi}=0.35$, $\theta=3.5$, and $K=1.5$ along with the experimental parameters listed in Table I. The "chi" parameter in Table I was calculated using the following relationship: $\chi_{aa}=A+B/T$, where $A=0$. The parameter B (=4.2) was calculated based on the numbers of statistical segments of PEO and DA (corresponding to the degree of polymerization of each constituent) at a critical temperature of 323 K. The values of χ_{ca} and χ_{ac} were obtained from the respective heat of fusion of each constituent using the approach of Rathi *et al.*[19] Equations (14)–(16) are simultaneously solved in dimensionless units for crystal order parameter, concentration, and thermal fields, but only the pattering forming aspects of crystal order parameter and the corresponding concentration fields were shown.

First, the dynamic calculation was carried out under a linear photointensity gradient, as shown in Fig. 2. Concentration fluctuations were generated by imparting thermal noise randomly in the whole picture frame including the edges. The computation box was subjected to a linear intensity profile with low intensity to the left and the high intensity to the right. The DA monomer is converted to polymer at a faster rate in the high intensity region (right side) relative to low light intensity region (left side), thereby raising the melting temperature of PEO rapidly above the reaction temperature and thus crystal nucleation occurs earlier and faster. However, the light intensity on the left side of the computation box is virtually zero, thus crystallization of DA cannot occur at that side. There are two opposing effects of heat liberations on the crystal growth behavior of PIC: the latent heat release by the growing crystal front of the crystalline PEO constituent and the heat of polymerization liberated in the polymerizing amorphous DA network. The heat of polymerization thus released would suppress the UCST coexistence curve and also could melt the growing crystals in close vicinity. Hence, the crystal growth front must propagate away from the polymerizing amorphous network region, thereby promoting the solid-liquid phase segregation over liquid-liquid phase separation.

The initial crystal structure thus formed is similar to a seaweed type growing epitaxially from the edges of the high intensity side. In directional solidification of crystals, the basic patterns can be classified into two types: "dendrites" and "seaweeds." A structure with pronounced orientational order is known as dendrite, and without apparent orientational order, it is called seaweed. The dendritic shape is a symmetric needle crystal with a parabolic tip, the sides of which are

TABLE I. Experimental and materials parameters of PEO/DA blends and the corresponding dimensionless model parameters used in the numerical computations.

Phase diagram calculation		Dynamic calculation	
$r_1=110$		$\widetilde{\Gamma^{\psi}}=10$	$W_1=6.76$
$r_2=1$	$\chi_{aa}=0.013$ at $T_r=323$ *K*	$\widetilde{\kappa^{\psi}}=0.35$	$\Delta H_P=86.25$ kJ/mol
$T_m=338$ *K*	$\chi_{ca}=0.27$ at $T_r=323$ *K*	$\widetilde{\theta}=3.15$	$\Delta H_{u,1}=8.36$ kJ/mol
$T_r=323$ *K*	$\chi_{ac}=0.01$ at $T_r=323$ *K*	$\widetilde{K}=1.35$	$k=0$, $k=0.2$ corresponding to minimum and maximum intensity
		$a_k=10^{-6}$ *m*	$D_k=10^{-11}$ m^2/s

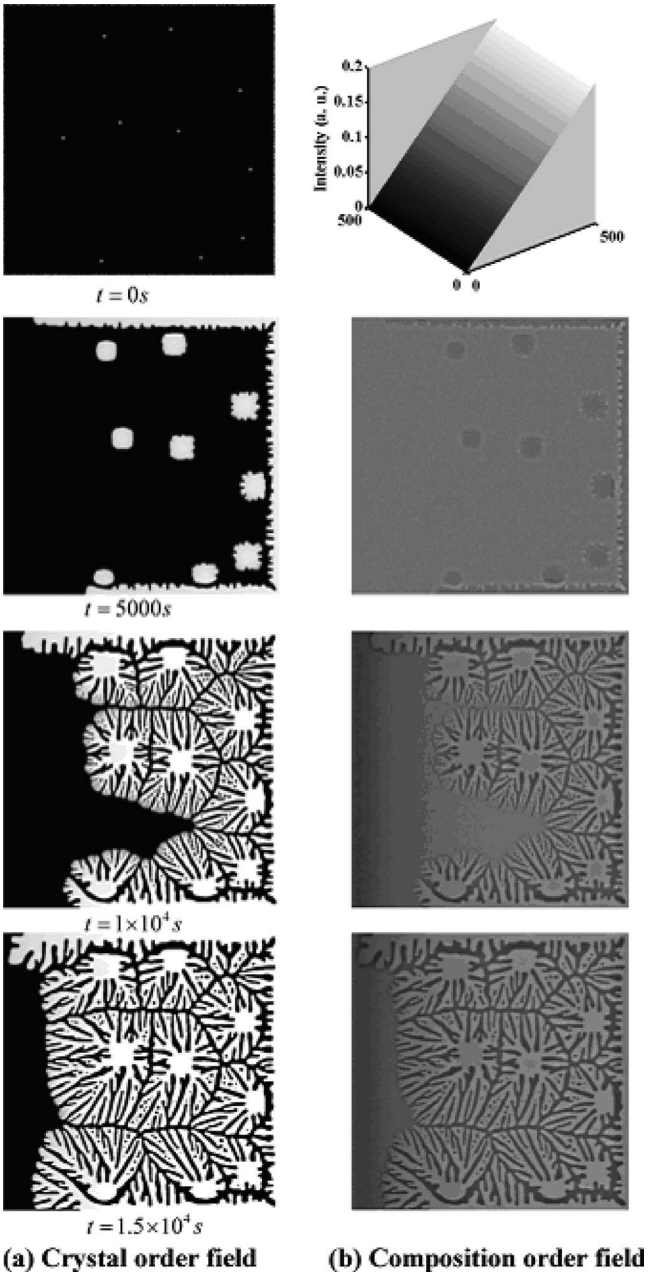

FIG. 2. Directional crystal growth showing seaweed growth from the frame and dense branching morphology (or spherulites) in the bulk: (a) the crystal order parameter field and (b) the corresponding composition order parameter field following PIC under a linear gradient illuminating beam. Note that the intensity of illuminating beam is the lowest at the left ($x=0$) and highest on the right side ($x=500$). The frame of the calculated patterns corresponds to the square grid of 500×500 μm^2. The dimensionless parameters used in this dynamic calculation along with the materials parameters were listed in Table I.

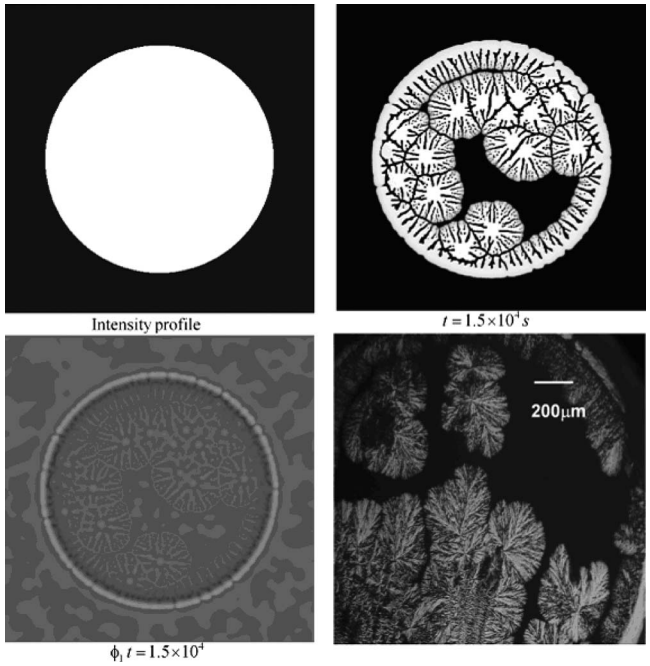

FIG. 3. Dynamic calculations carried out under a circular light intensity profile. The sharp transition of the interface from the high intensity to low intensity interface region leads to directional crystal growth toward the high intensity center and no crystal growth was observable in the dark region due to the lack of the photoreaction. The last picture at the bottom right shows the observed morphology of the 30/70 PEO/DA blend, showing directional crystal growth under the polarized optical microscopic view. The computed picture frame corresponds to 500×500 μm^2.

influenced by a secondary branching. The seaweed morphology is characterized by repeating tip splitting at the advancing crystal front.[27,28]

With the progression of the photoreaction, more nuclei are formed in the intermediate region as the photopolymerization catches up to that of the high intensity region. These nuclei grow through tip splitting and branching and eventually evolved to dense spherulitic morphology. Some dark spots can be noticed suggesting that some traces of solvents are trapped in these growing crystals. With continued reaction, the differential crystal growth behavior can be seen clearly on both upper and lower sides, i.e., the seaweed growth is faster on the higher intensity side relative to the lower intensity side. This directional crystal growth is similar to those observed in succinonitrile subjected to temperature gradients in which a linear temperature gradient was applied to the experiment creating gradient in the supercooling (i.e., the driving force for crystallization).[27]

Figure 3 shows the simulated morphology under a cylindrical intensity profile of the incident light with a flattop that drops discretely at the circumference. Several nuclei were triggered through the crystal density fluctuations at the circular boundary as well as inside the circular beam. Concurrently, concentration fluctuations were generated randomly over the entire computation frame. As mentioned earlier, the reaction rate depends on the intensity of illuminating beam. Since the intensity is uniform at the flat circular top, polymerization driven crystallization can occur at the circumference and the inner side almost simultaneously. As can be seen in the crystal order parameter field, the epitaxial crystal growth occurs from the circular boundary inwards directionally. As can be seen in the right picture of the upper row of Fig. 3, the interface morphology thus developed seems to be a seaweed type.[28] Moreover, there appear some crystals growing radially from several common nuclei through branching and tip splitting leading to the dense branching morphology in metals or spherulites in crystalline polymers. A similar pattern, but somewhat faint, can be discerned in the concentration field (the middle picture of the bottom row). The simulated growth pattern (the left bottom row) is strik-

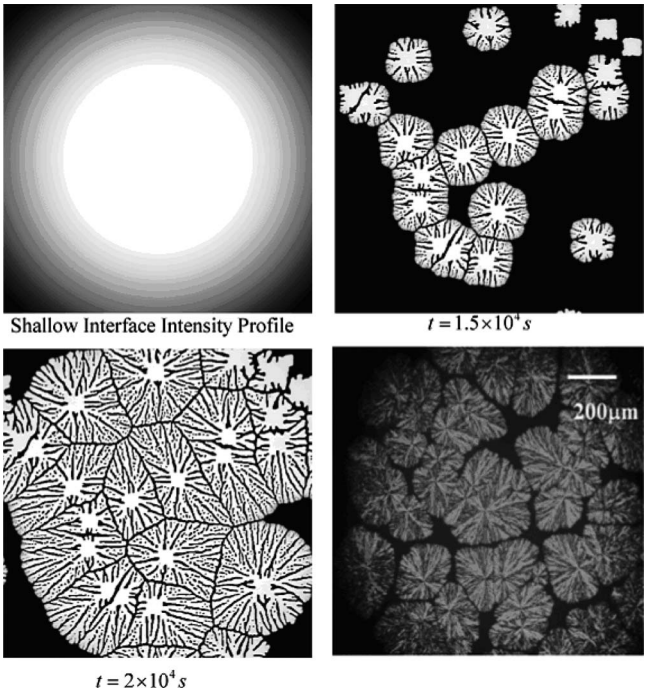

FIG. 4. Dynamic calculations carried out under a smooth Gaussian intensity profile revealed a faster growth in the high intensity core region vs slower growth in the low intensity region in the outer area. The entire view area was filled with dense branching morphology (or spherulites) as they grew in the entire domain as the monomer was converted in to polymer. The last picture at the bottom row shows the optical micrograph of the emerged spherulitic morphology from the 30/70 blend of PEO/DA. The light intensity has a Gaussian profile after passing through a set of convex lens. The computed picture frame corresponds to 500×500 μm^2.

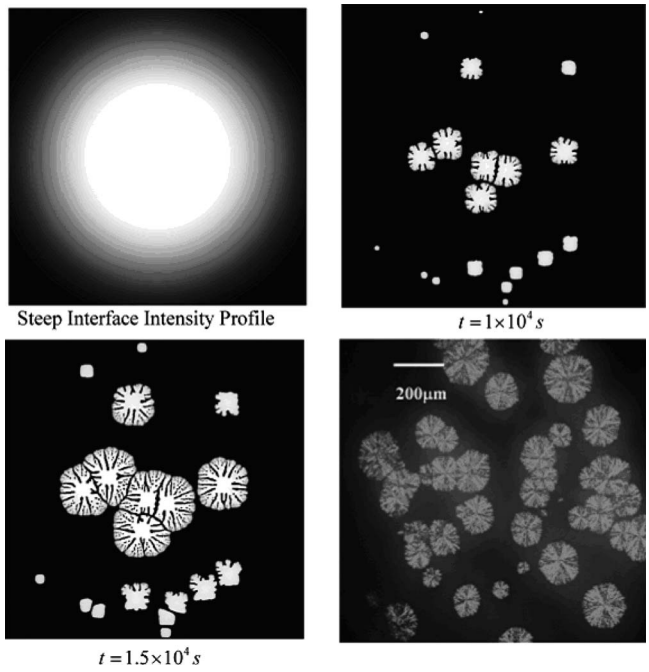

FIG. 5. Dynamic calculations carried out under a sharper Gaussian intensity profile showing crystallization in the high intensity region and directional crystal growth from the low intensity region toward the core of high intensity region. The last picture at the bottom row shows the optical micrograph of the emerged spherulitic morphology from the 30/70 blend of PEO/DA. The computed grid corresponds to 500×500 μm^2.

ingly similar to the PEO crystal patterns of the 30/70 PEO/DA blend (the right picture in the bottom row) exposed to the green light at 50 °C under the cross-polar configuration.

Now we shall examine crystal growth under a Gaussian intensity profile with a shallow smooth interface,[10] in which the intensity decays away gradually from the highest intensity at the center (Fig. 4). Experimentally, this beam profile may be created by defocusing the incident light with the aid of a set of converging lens and a circular orifice in front of the blend sample. However in contrast to the flat circular top profile, the light intensity decays gradually from the center with a smooth interface and thus there is a sharp intensity contrast for the crystals to grow directionally. Hence the dense branching morphology or polymer spherulites develop and grow predominantly near the center accompanied by smaller spherulites at the peripherals. The observed distribution of spherulite sizes is not surprising in view of the fact that the polymerization at the peripheral (i.e., the lower intensity side) is slow and thus the crystal at the peripheral nucleates late relative to those at the center, but it eventually catches up with those at the center with continued progression of the reaction. This simulated crystal morphology can be confirmed experimentally in the 30/70 PEO/DA blend showing distribution of large PEO spherulites in the center surrounded by smaller ones at the peripheral.

Another calculation was carried out using an intensity profile, which is intermediate between the circular-sharp and shallow Gaussian interfaces, showing a steep but smooth Gaussian profile (Fig. 5). The crystal nucleation is heterogeneous showing a larger growth in the high intensity region relative to the smaller ones at the interface. In the intensity at the tail end of the beam is the lowest, thus any crystals thus nucleated probably disappear. The present calculation revealed that the crystal growth was dominant in the high intensity region over the low intensity region.

To experimentally verify the above simulated gradient morphology, the 30/70 PEO/DA blend was exposed to a defocused green light. The optical micrograph obtained under the cross-polar configuration is depicted on the right of the bottom row of Fig. 5. The observed spherulitic morphology of PEO and its size distribution are in reasonably good agreement with the simulated patterns. Figure 6 shows a set of the merged spherulitic morphologies of sharp circular, Gaussian profile with a shallow smooth interface, and their intermediate profile with a steep smooth interface. This comparison clearly shows that the interface intensity profile (i.e., the interface sharpness of the illuminating beam) exerts profound influence on the behavior of the PIC. The corresponding experiments of the PEO/DA blends lend support the present calculated trends, illustrating the effect of photointensity gradients and the interface sharpness on the dense branching lamellar (or spherulitic) morphology undergoing PIC. The region with a dark appearance within the interlamellar regions of the spherulites may be attributed to the trapped DA solvent, which may be a consequence of liquid-liquid phase separation. It is reasonable to infer that the heat of polymerization liberated from the polymerizing DA network can melt away the growing crystals which are in the

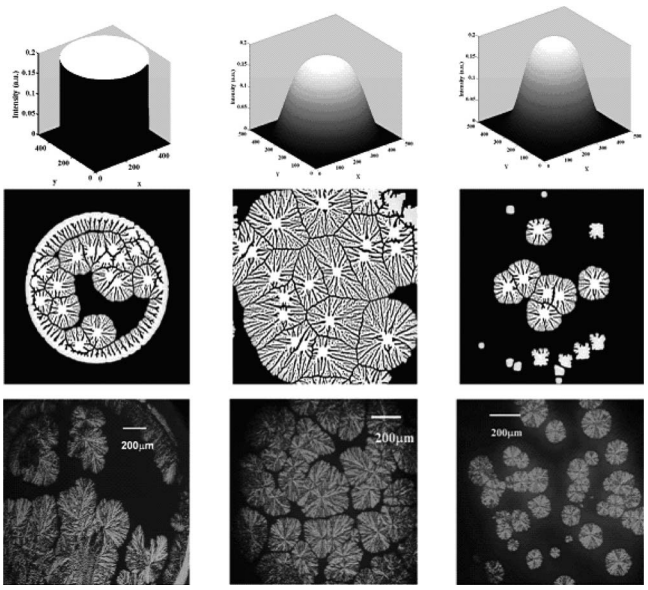

FIG. 6. Comparison among crystallization in polymer blends undergoing polymerization when exposed to circular, slowly decaying Gaussian profile and a sharp Gaussian profile. Note that the directional crystal growth is dependent on the intensity profile and the sharp Gaussian profile is an intermediate between the circular profile having sharp interface in which the growth advances directionally toward the high intensity region, as opposed to the gradual smooth Gaussian profile in which crystals grow away from the high intensity core. The computed picture frame corresponds to 500 $\times 500$ μm^2.

close vicinity. Hence, the crystal growth front must propagate away from the polymerizing high intensity region exhibiting the coexistence of PEO spherulites in the continuum of acrylate networks, which is a signature of solid-liquid phase segregation.

IX. CONCLUSIONS

We have demonstrated the effects of intensity gradient on gradient crystalline morphology undergoing PIC in the PEO/DA blends. The interface sharpness of the incident beam creates a gradient in the polymerization rate leading to the directional crystal growth such as seaweed. The directional seaweed growth leading to the dense branching morphologies (or spherulites) of the PEO/DA blends driven by photointensity gradient are consistent with the present theoretical calculations. The lack of liquid-liquid phase separated structure in the matrix of the polymerizing PEO/DA system may be attributed to the heat of polymerization liberated from the polymerizing DA network, which probably suppresses liquid-liquid phase separation. Moreover, this reaction heat can melt away the growing crystals that are in the close vicinity and thus the crystal growth front must propagate away from the polymerizing high intensity region, thereby showing predominantly the behavior of solid-liquid phase segregation.

ACKNOWLEDGMENTS

Support of this work by the National Science Foundation through Grant No. DMR-0514942 is gratefully acknowledged.

[1] *Rubber Toughened Plastics*, Advance Chemical Series, edited by C. K. Riew (American Chemical Society, Washington, DC, 1989), Vol. 222.
[2] R. J. Williams, B. A. Rozenberg, and J.-P. Pascault, Adv. Polym. Sci. **128**, 95 (1997).
[3] *Heterophase Network Polymers*, edited by B. A. Rozenberg and G. M. Sigalov (Taylor & Francis, New York, 2002).
[4] T. Inoue, Prog. Polym. Sci. **20**, 119 (1995).
[5] T. Kyu and J. H. Lee, Phys. Rev. Lett. **76**, 3746 (1996).
[6] J. Y. Kim, C. H. Cho, P. Palffy-Muhoray, M. Mustafa, and T. Kyu, Phys. Rev. Lett. **71**, 2232 (1993).
[7] D. Nwabunma, H.-W. Chiu, and T. Kyu, Macromolecules **33**, 1416 (2000).
[8] D. Nwabunma, H.-W. Chiu, and T. Kyu, J. Chem. Phys. **113**, 6429 (2000).
[9] S. Park, P. Rathi, and T. Kyu, Phys. Rev. E **75**, 051804 (2007).
[10] J. D. Gunton, M. San Miguel, and P. S. Sahni, in *Phase Transitions and Critical Phenomena*, edited by C. Domb and J. L. Lebowitz (Academic, New York, 1983), Chap. 3.
[11] V. Ferreiro, J. F. Douglas, J. A. Warren, and A. R. Karim, Phys. Rev. E **65**, 042802 (2002).
[12] P. J. Flory, *Principles of Polymer Chemistry* (Cornell University Press, Ithaca, 1953).
[13] R. Kobayashi, Physica D **63**, 410 (1993).
[14] T. Kyu, R. Mehta, and H. W. Chiu, Phys. Rev. E **61**, 4161 (2000).
[15] R. Mehta, W. Keawwattana, A. L. Guenthner, and T. Kyu, Phys. Rev. E **69**, 061802 (2004).
[16] H. Xu, R. Matkar, and T. Kyu, Phys. Rev. E **72**, 011804 (2005).
[17] H. Xu, W. Keawwattana, and T. Kyu, J. Chem. Phys. **123**, 124908 (2005).
[18] R. A. Matkar and T. Kyu, J. Phys. Chem. B **110**, 12728 (2006).
[19] P. Rathi, T.-M. Huang, P. Dayal, and T. Kyu, J. Phys. Chem. B **112**, 6460 (2008).
[20] G. R. Tryson and A. R. Shultz, J. Polym. Sci., Polym. Phys. Ed. **17**, 2059 (1979).
[21] C. Decker and K. Moussa, Makromol. Chem. **189**, 2381 (1988).
[22] K. S. Anseth, C. M. Wang, and C. N. Bowman, Macromolecules **27**, 650 (1994).
[23] E. Andrzejewska, Macromol. Symp. **171**, 243 (2001).
[24] H. Duran, S. Meng, N. Kim, J. Hu, T. Kyu, L. V. Natarajan, V. P. Tondiglia, and T. J. Bunning, Polymer **49**, 534 (2008).
[25] P. Rathi and T. Kyu, Phys. Rev. E **79**, 031802 (2009).
[26] S. J. Park and T. Kyu, Macromolecules **42**, 1180 (2009).
[27] T.-M. Guo, H.-J. Xu, T. Kyu, and G.-X. Wang, in *TMS Symposium Proceeding*, edited by M. Rappaz, C. Beckermann, and R. Trivedi (The Minerals, Metals & Materials Society, Warrendale, 2004), Vol. 393.
[28] H. Xu, Ph.D. dissertation, "Morphology landscape under unidirectional solidification," University of Akron, May 2004.